Energy Disposal in the Photodissociation of $Co(CO)_3NO$ near 225 nm

Jeffrey A. Bartz,† Tyson O. Friday, Brian R. Goodman, Steven E. Kooi, Richard G. Blair, and William F. Polik*

Department of Chemistry, Hope College, Holland, Michigan 49423

Received: July 16, 1998; In Final Form: October 20, 1998

The photodissociation of $Co(CO)_3NO$ was studied near 225 nm. Apparent two-photon dissociation of the parent compound produces Co* in a number of excited states that emit in the range of 340−360 nm. Both quartet and doublet states of Co* are observed, implying the existence of spin-conserving and nonspin-conserving dissociation channels. Assignment of the Co* emission is used to calculate an upper limit for the average metal−ligand bond dissociation energy of 36.2−38.6 kcal/mol with no spin-conservation restrictions and 41.2−43.9 kcal/mol with spin-conservation restrictions. The Co* emission intensities are used to determine the relative populations of particular *J* and spin states and to demonstrate that *J* states within a particular LS configuration are statistically populated. The NO photoproduct was detected by fluorescence excitation spectroscopy. The NO appears to follow dual Boltzmann statistics with rotational temperatures of 580 ± 70 K for $E_{rot} < 500$ cm^{-1} and 2800 ± 300 K for $E_{rot} > 500$ cm^{-1}.

I. Introduction

The photodissociation dynamics of organometallic compounds provide information about coordinatively unsaturated intermediates. These unsaturated intermediates are important in catalysis and are also becoming increasingly important in material deposition processes. Herein we describe an investigation of the emission spectroscopy, both by fluorescence excitation and dispersed fluorescence detection, of the products from the gas-phase photodissociation of tricarbonylnitrosylcobalt, $Co(CO)_3NO$.

$Co(CO)_3NO$ has been studied previously. Zink and co-workers performed gas-phase photochemical experiments that revealed that the Co−NO bond bends after $Co(CO)_3NO$ is excited near 400 nm.[1] Rayner et al. found that 248-nm photolysis of $Co(CO)_3NO$ generates CoCO as a one-photon dissociation product using transient infrared spectroscopy.[2] Wang et al. have more recently studied the photodissociation of $Co(CO)_3NO$ at 355 and 266 nm by transient infrared spectroscopy.[3] In their analysis, one-photon photodissociation of $Co(CO)_3NO$ at 266 nm produces $Co(CO)_2$ and other products. Wight and co-workers have studied the photofragments from the photodissociation of $Co(CO)_3NO$ by resonance-enhanced multiphoton ionization (REMPI).[4−6] Near 225 nm, they found two temperatures in the NO photofragment rotation, 450 and 1400 K.[4] In the 450-nm spectral region, Wight observed that the NO rotational distribution from the photodissociation of $Co(CO)_3NO$ displays a non-Boltzmann character, which was interpreted as NO dissociating via an impulsive mechanism.[5] Further REMPI experiments investigating the bare Co atom following photodissociation[6,7] found that the Co product distribution depended on the size of a substituted ligand and the laser power near 450 nm.[6] Hellner et al. have studied the vacuum UV photodissociation of $Fe(CO)_5$, $Ni(CO)_4$, and $Co(CO)_3NO$ by observing the emission of excited metal atoms.[8] They used these data to estimate the total bond dissociation energies in each of the compounds.

This contribution uses dispersed fluorescence (DF) and fluorescence excitation (FE) spectroscopies to study an apparent two-photon photodissociation of $Co(CO)_3NO$ near 225 nm. DF was used to determine the nascent Co* product distribution following the multiphoton dissociation of $Co(CO)_3NO$. FE permitted the determination of the NO photoproduct rotational energies.

Several authors have used DF to detect metals or FE to detect ligand photofragments.[9−17] For example, one of the earliest reports of gas-phase organometallic chemistry was that of Karny et al. in which they observed metal emission from several metal-containing compounds by DF.[9] Later reports used the DF technique to understand the bonding interactions and photodissociation dynamics of many organometallic compounds.[14−17] FE has been used to investigate ligands, such as CO, following the photodissociation of organometallic complexes.[18−21] For example, Schlenker et al. used FE to determine the rotational, vibrational, and translational energies of CO following the photodissociation of $Ni(CO)_4$.[21] Other metal carbonyls have been studied by this method.[18−20]

II. Experimental Section

$Co(CO)_3NO$ (Strem Chemicals) was stored in a freezer or in liquid nitrogen between experiments. The compound was purified by three freeze−pump−thaw cycles before use. A neat $Co(CO)_3NO$ sample was introduced into the experimental apparatus by room-temperature vacuum transfer. NO (Matheson) was used without further purification.

Figure 1 schematically represents the experimental setup. The neat $Co(CO)_3NO$ sample flowed into a pulsed nozzle (General Valve Series 9) with a 0.030-in. orifice. The pulsed nozzle was driven by a 200-μs, 180-V pulse that admitted a 600-μs pulse of gas into the vacuum chamber. The chamber was pumped by a 6-in. diffusion pump (Edwards Diffstak 160) backed by a 10 L/s roughing pump.

The laser light was produced by an excimer-pumped dye laser system (Lambda Physik EMG 101/FL2001) using Coumarin 440. The dye output was doubled in a BBO crystal (Quantum

* To whom correspondence should be addressed. E-mail: polik@hope.edu.
† Present address: Department of Chemistry, Kalamazoo College, Kalamazoo, MI 49006-3295. E-mail: jbartz@kzoo.edu.

10.1021/jp983056c CCC: $15.00
Published on Web 12/05/1998

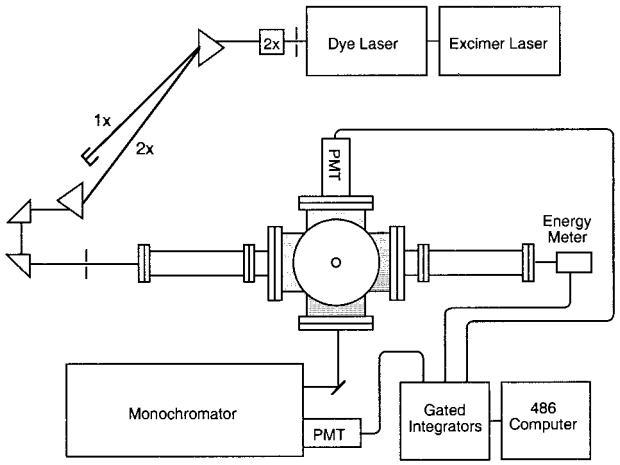

Figure 1. Experimental layout for dispersed fluorescence and fluorescence excitation studies of $Co(CO)_3NO$.

Technology), and 40−70 μJ of doubled light was separated from the fundamental by two 60° quartz prisms. The 10-ns pulses of laser light were approximately 2-mm square and remained unfocused in these experiments. The energy density was approximately 0.4−0.8 mJ/cm^2. The laser power was monitored with a pyroelectric detector (Molectron J4-09) connected to an energy meter (Molectron J1000).

Dispersed fluorescence spectra were recorded by fixing the laser wavelength, collecting the fluorescence with a 12-in. focal length (fl) quartz lens, directing the fluorescence through light baffles with a pair of mirrors, and imaging the fluorescence with a 8-in. fl quartz lens into a 1.25-m monochromator (Spex 1250M) with a 2400 grooves/mm grating. The heights of the entrance and exit slits were 1 cm, and the widths were 125 μm. The dispersed fluorescence was detected with a photomultiplier tube (PMT) (Thorn EMI 9954QB) mounted behind the exit slit of the monochromator. The fluorescence signal from the PMT was averaged by a gated integrator with a 30-ns delay and a 150-ns width. The total fluorescence and laser power were simultaneously measured.

Fluorescence excitation was monitored with a PMT (Thorn EMI 9954QB) situated at right angles to both the laser and molecular beam axes. A 30-nm band-pass filter (Janos XB02) was used to remove spontaneous fluorescence from Co atoms (section III.B). The induced NO fluorescence signal was averaged with a gated integrator (Stanford Research Systems SR250), digitized (Keithley Metrabyte DAS8-PGA), and stored on a 486 computer. The gate widths were typically 150 ns and delayed 100 ns after the laser pulse. Additional gated integrators, with 15−50-ns delays and 10−20-ns gate widths, were used to identify induced fluorescence from Co atomic lines (section III.B). Another gated integrator averaged the output of the laser energy monitor, which was digitized and stored along with the signals.

Lifetime measurements of several spectral features (section III.B) were determined by recording the fluorescence with a digital oscilloscope (Tektronix TDS540) interfaced to the 486 computer. The fluorescence signal was averaged for 100 shots, digitized, and stored. The lifetimes were determined by fitting the decays to a single exponential on a Macintosh computer using IGOR (WaveMetrics).

III. Results

A. Dispersed Fluorescence Spectrum of Nascent Co. The dominant fluorescence feature following the photodissociation of $Co(CO)_3NO$ is emission from the nascent Co* states produced by multiphoton dissociation of the parent compound. A DF spectrum of Co* emission following 221.5-nm photodissociation appears in Figure 2. The assignments for the observed transitions also appear in Figure 2 and are discussed in section IV.A. Figure 3 contains a power-dependence determination for the most intense feature in Figure 2, $a^4F_{9/2} \leftarrow z^4G_{11/2}$ at 346.580 nm. The slope of the log−log plot indicates a power dependence of 2.08 ± 0.26, implying that this feature arises from a two-photon process.

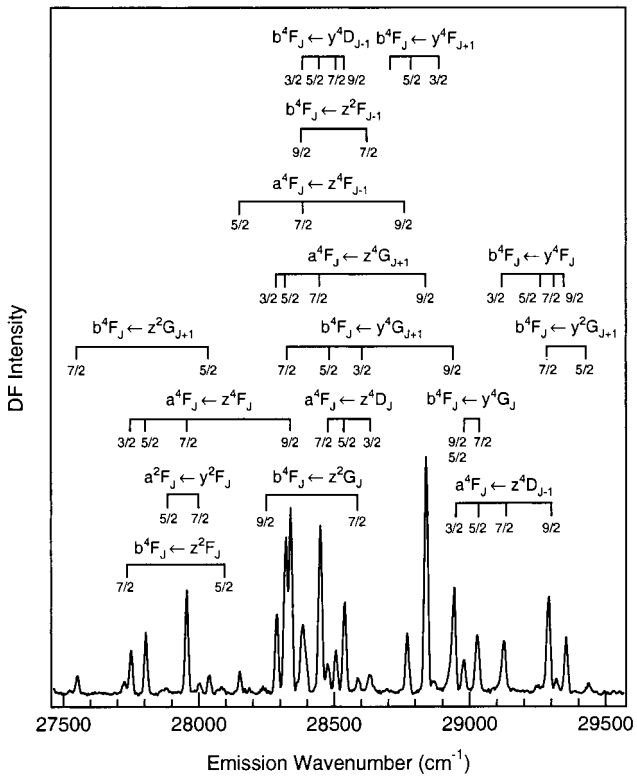

Figure 2. Nascent Co* dispersed fluorescence emission spectrum from the 221.5-nm photodissociation of $Co(CO)_3NO$.

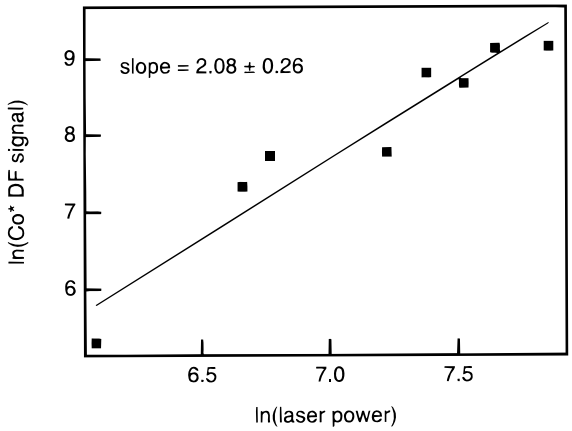

Figure 3. Power dependence of Co* product fluorescence from the 221.5-nm photodissociation of $Co(CO)_3NO$. The line is a linear least-squares fit to the data with a slope of 2.08 ± 0.26, implying that two photons are required to fully dissociate $Co(CO)_3NO$.

B. Fluorescence Excitation Spectrum of NO. Because the most intense feature in the emission spectrum following the photodissociation of $Co(CO)_3NO$ arises from the spontaneous emission from nascent Co* atoms around 340−360 nm, a 30-nm band-pass filter centered at 250 nm was used to block spontaneous Co* emission and transmit the induced NO

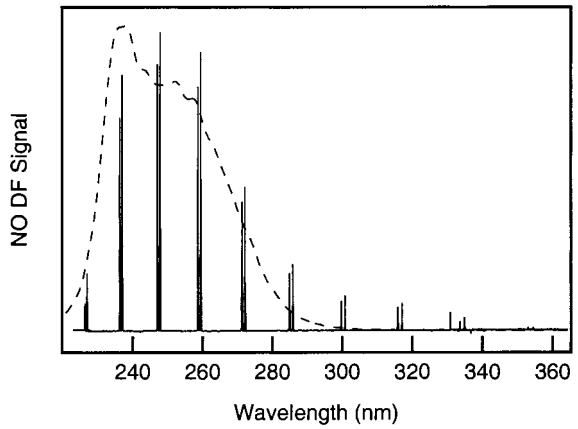

Figure 4. Dispersed fluorescence of room-temperature NO (solid line). The transmission curve of the band-pass filter used to record fluorescence excitation spectra of NO while discriminating against emission from nascent Co* atoms around 340−360 nm in these experiments is overlaid (dashed line).

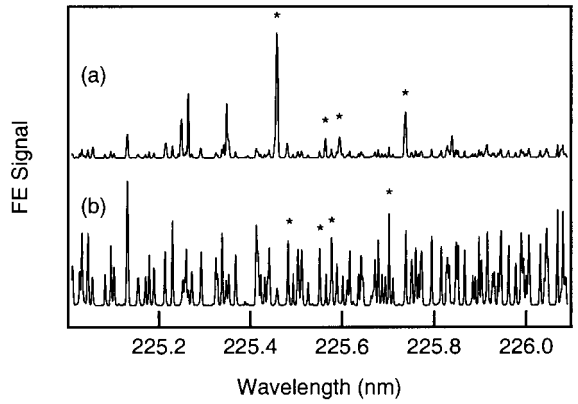

Figure 5. Comparison of intensity of features in the fluorescence excitation spectrum following the photodissocation of $Co(CO)_3NO$ as a function of gated integrator delay and gate width. The upper data (a) have a 15-ns gate delay and a 20-ns gate width. The lower data (b) have a 100-ns gate delay and a 150-ns gate width. Lifetime measurements were recorded of peaks marked with asterisks.

fluorescence. Figure 4 shows the transmission curve of the 30-nm band-pass filter superimposed on the dispersed fluorescence spectrum of room-temperature NO excited at 226.17 nm via the $P_{12}(4.5)$ transition.

Induced fluorescence from the direct laser excitation of Co atoms, following the complete dissociation of all of the ligands from $Co(CO)_3NO$, overlaps with the induced fluorescence of NO in the FE spectrum. These induced Co emissions have much shorter lifetimes than the induced NO fluorescence. Figure 5 shows a comparison of the fluorescence detected by different gating schemes. In the upper spectrum, Figure 5a, the gate delay was 15 ns and the gate width was 20 ns. In the lower spectrum, Figure 5b, the gate delay was 100 ns and the gate width was 150 ns. Comparison of the two spectra gives an indication of the lifetimes of the dominant features within each spectrum. Large features in the top spectrum arise from species with shorter emission lifetimes, relative to the lifetimes of features in the bottom spectrum. DF experiments confirmed that the short-lived induced fluorescence came from laser-excited Co atoms and the long-lived fluorescence came from NO FE. The induced fluorescence of Co atoms appeared between 220 and 300 nm, at a higher photon energy than the spontaneous fluorescence of the nascent Co* photoproducts, which appeared between 340 and 360 nm. The emission lifetimes of certain

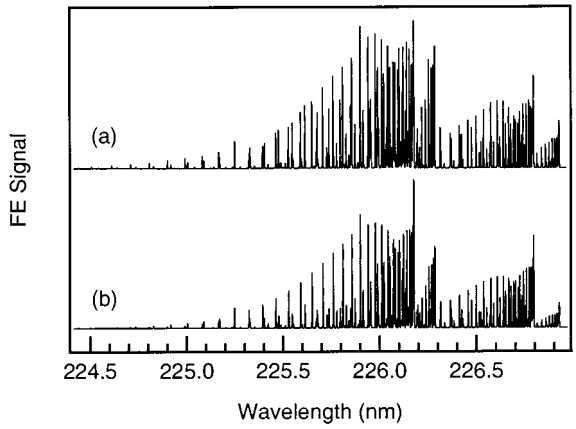

Figure 6. (a) Fluorescence excitation spectrum of pure NO at room temperature and (b) calculated fluorescence excitation spectrum NO at 295 K.

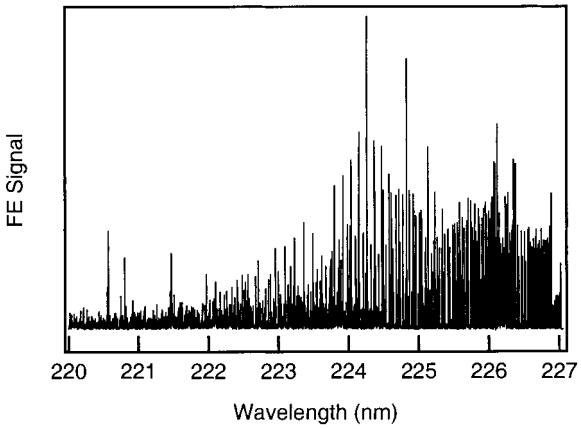

Figure 7. Fluorescence excitation spectrum of NO from the photodissociation of $Co(CO)_3NO$. The photolysis and excitation occur in the same laser pulse; thus, the wavelength for each process is the same.

emission features, highlighted by asterisks, were determined. The lifetime average for the Co features in the upper spectrum is 12.3 ± 4.8 ns. In comparison, the lifetime average for the NO features in the lower spectrum is 190.3 ± 5.6 ns. A 100-ns gate delay allowed the preferential observation of the NO features in the FE spectrum, relatively unobscured by the short-lived Co features.

The room-temperature FE spectrum of pure NO appears in Figure 6a. This spectrum was used to calibrate the emission intensities and to check the validity of a calculated NO FE spectrum.[22,23] The NO FE spectrum was calculated for the NO $A(v'=0) \leftarrow X(v''=0)$ transition at 295 K and appears in Figure 6b.

Figure 7 contains the FE spectrum of NO following the photodissociation of $Co(CO)_3NO$. Because this is a one-laser experiment, the wavelengths used for photodissociation and FE of NO are the same. This spectrum is normalized to the apparent laser power dependence. Figure 8 shows a laser-power-dependence determination for NO FE, which indicates a power dependence of 1.88 ± 0.05. Power dependences of the NO signal varied from 1.6 to 1.9, suggesting a partial saturation of one or both of the excitation steps. At 225 nm, the absorption cross section of $Co(CO)_3NO$ ($\sigma \sim 10^{-16}$ cm^2)[1] is 3 orders of magnitude larger than NO ($\sigma \sim 10^{-19}$ cm^2).[24] Because of the differences in absorption cross sections, the photodissociation step will be more likely to saturate as compared to the fluorescence excitation of NO.

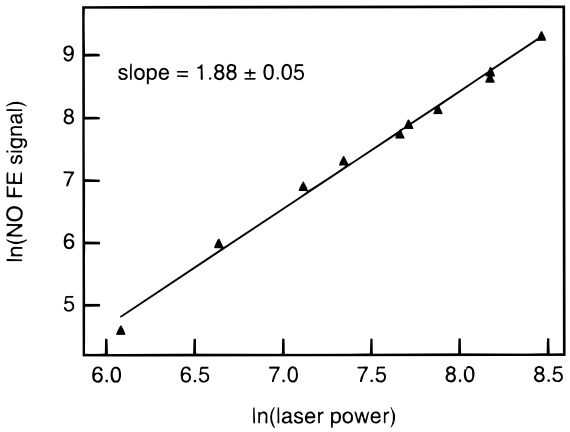

Figure 8. Power dependence of NO fluorescence excitation following the photodissociation of $Co(CO)_3NO$. The line is a linear least-squares fit with a slope of 1.88 ± 0.05, implying that $Co(CO)_3NO$ absorbs one photon to dissociate NO and then NO absorbs a second photon in the fluorescence excitation step.

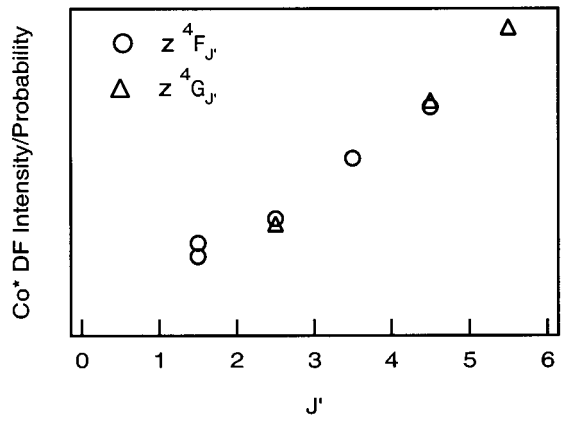

Figure 9. Relative populations of nascent Co* atoms determined by comparison of the fluorescence intensities normalized by the emission probability. The linear dependence arises from statistical population of the $2J' + 1$ degenerate LS states.

IV. Discussion

A. Co* Product Assignments. The DF spectrum of the nascent Co* population permits assignment of 47 atomic transitions.[25] These assignments, grouped into 16 different progressions between the excited and ground states, appear in Figure 2. Many of the features in the DF spectrum result from the overlap of more than one transition. A plot of ln(emission intensity/degeneracy) versus upper state energy for the nascent Co* product populations did not yield a distribution that could be fitted by a single line, which would correspond to a Boltzmann temperature. However, an analysis of the relative populations of the z^4G and z^4F excited states, in which multiple emission features were observed that were not overlapped with other transitions, reveals a linear dependence on J. Figure 9 shows that these relative populations are fully consistent with the $2J + 1$ degeneracy of a given state and implies a statistical population of the nascent Co* photoproduct J levels within a particular LS state.

It is readily apparent in Figure 2 that the relative populations of excited quartet states are much higher than the doublet states, in the nascent Co* product distribution. Spin conservation during the dissociation or formation of organometallic compounds has been an important question.[6,26−28] Depending on the ligands and metal, spin changes provide alternate pathways for successive additions or subtractions of ligands. Armentrout and Wight's photodissociation/REMPI experiments with $Co(CO)_{3-x}(PR_3)_xNO$ ($x = 0$ or 1, R = CH_3, n-C_3H_7, or n-C_4H_9) near 450 nm have revealed that at low laser powers or with large R groups, doublet states of Co are produced.[6,29] Because the parent molecules are all singlets, the CO ligands are singlets, and the NO is a doublet, spin is conserved in the dissociation when the Co product is in a doublet state. However, Armentrout and Wight found that spin is not conserved at higher photon flux, as the excited molecule is able to access higher energy, nonspin-conserving dissociation channels to produce Co products in quartet states. They suggested that the higher photon flux increases the photon absorption rate, relative to the photodissociation rate, and results in more photons absorbed and a higher internal energy within the molecule and its fragments. The 221.5-nm photolysis here provides further evidence for the failure of spin conservation at higher internal energies. The 221.5-nm photons, with approximately twice the energy per photon than the 445-nm photons used by Armentrout and Wight, supply a total photon energy that is at least 97.6 kcal higher than the threshold adiabatic BDE, as discussed in section IV.B below. With this high amount of excess internal energy, the dissociating fragments are able to cross from a low-spin doublet to a high-spin quartet dissociation channel.

B. Bond Dissociation Energy from Emission Wavelengths. One of the pieces of information revealed by the analysis of the DF spectrum is an upper limit for the sum of the metal−ligand bond dissociation energies (BDEs). The sum of the BDEs in $Co(CO)_3NO$ is related to the energy difference between the photons absorbed by the complex and those emitted by the Co* atom. From power-dependence measurements, there is an apparent two-photon power dependence for the complete photodissociation of $Co(CO)_3NO$ to produce the nascent Co* product (Figure 3). Analysis of the emission frequencies from Co* allows the determination of the excited states and energy levels of the nascent metal product. Two 221.5-nm photons deliver 258.2 kcal/mol to $Co(CO)_3NO$, and the highest excited state assigned in Figure 2 is $y^2F_{5/2}$ at 36 300 cm^{-1} (103.8 kcal/mol). The difference between these two values, 154.4 kcal/mol, represents the energy available for the dissociation of the three Co−CO bonds and one Co−NO bond in $Co(CO)_3NO$ and corresponds to an average adiabatic bond dissociation energy of 38.6 kcal/mol. It is significant that a higher energy state does not appear in the spectrum. Specifically, the $b^4F_{9/2} \leftarrow x^4D_{7/2}$ transition, at 36 166 cm^{-1} (2764.19 Å), is absent from the dispersed fluorescence spectrum of the nascent Co* product, although quartet-to-quartet transitions have the highest intensity in the DF spectrum. This transition, however, is present in the photodissociation of $Co(CO)_3NO$ at higher total photon energies.[30] There is not enough energy in two 221.5-nm photons to dissociate $Co(CO)_3NO$ and produce Co* in the $x^4D_{7/2}$ state at 39 649 cm^{-1} (113.4 kcal/mol), although there is sufficient energy to produce the $y^2F_{5/2}$ at 36 300 cm^{-1}. Thus, the average bond dissociation energy cannot be any smaller than 36.2 kcal/mol. Such an estimate of the adiabatic BDE neglects the internal energy of the photodissociated ligands and their translational energy, and it does not assume spin conservation during dissociation of $Co(CO)_3NO$.

Spin conservation is an important consideration in defining metal−ligand bond dissociation energies. Fenske and Jensen assign the ground state of $Co(CO)_3NO$ as a singlet.[31] When the ligands dissociate, the three CO ligands will exit in singlet states and NO in a doublet state if spin is conserved. Thus, the bare Co atom from the dissociation of $Co(CO)_3NO$ should appear in a doublet state. Since the lowest energy doublet state ($a^2F_{7/2}$)

TABLE 1: Average Metal−Ligand Bond Dissociation Energies (M−L BDEs) in kcal/mol

compd	products	total BDE	av BDE	ref
$Co(CO)_3NO$	Co + 3CO + NO	144.8−154.4	36.2−38.6	this work[a]
$Co(CO)_3NO$	Co + 3CO + NO	164.6−175.7	41.2−43.9	this work[b]
$Fe(CO)_5$	Fe + 5CO	133 ± 22	26.6 ± 4.5	28[c]
$Ni(CO)_4$	Ni + 4CO	137.4 ± 8.5	34.4 ± 2.1	27
$Co(CO)_3NO$	Co + 3CO + NO	148−175	37−44	8[a]
$Co(CO)_3NO$	CoCO + 2CO + NO	115	38	2
$Co(CO)_3NO$	$Co(CO)_2$ + CO + NO	107	54	3

[a] Adiabatic dissociation to Co $a^4F_{9/2}$. [b] Diabatic dissociation to Co $a^2F_{7/2}$. [c] Adiabatic dissociation.

in Co is 7442.41 cm^{-1} above the ground state of Co ($a^4F_{9/2}$), the spin-conserving diabatic BDE is 21.3 kcal/mol greater than the adiabatic BDE. Thus, the average diabatic BDE in $Co(CO)_3NO$ is 41.2−43.9 kcal/mol. Table 1 summarizes these calculations. This estimate is an upper limit for the BDEs because it neglects the internal and translational energies of the photodissociated ligands.

The average adiabatic BDE in $Co(CO)_3NO$ determined here is larger than that average M−CO BDE for two first-row transition-metal carbonyls, $Fe(CO)_5$ and $Ni(CO)_4$, as determined by collisionally induced dissociation.[27,28] In this case, it is likely because the BDE of a linear metal−nitrosyl bond, as is found in $Co(CO)_3NO$, is larger than the BDE of a metal−carbonyl bond.[32] The estimate of the average adiabatic BDE found in these experiments (36.2−38.6 kcal/mol) is significantly narrower than the range of possible values for average BDEs determined by Hellner et al. from the vacuum UV photolysis of $Co(CO)_3NO$ (36.9−43.7 kcal/mol).[8] Rayner et al.[2] find that a one-photon photolysis of $Co(CO)_3NO$ at 248 nm forms CoCO. This indicates that the average adiabatic metal−ligand BDEs for the dissociation of two carbonyls and the nitrosyl is 38 kcal/mol. However, Wang et al.[3] argue that 248- and 266-nm photolyses of $Co(CO)_3NO$ form $Co(CO)_2$, citing the work of Hellner et al.[8] and suggesting that 248-nm photolysis to form CoCO provides little excess energy for the photoproducts. Their revised assignment of the primary one-photon product would raise the sum of the adiabatic BDE of one Co−CO bond and the Co−NO bond to 107 kcal/mol and the average BDE for these two bonds to 54 kcal/mol. More experimental work investigating the primary photodissociation products and their internal energy distributions is required to resolve the differences in these data.

C. NO Rotational Energy Distribution. The NO FE spectrum was analyzed by constructing Boltzmann plots of the peak intensities. The integrated intensity of a transition is

$$I = S \exp\left(-\frac{E_{rot}}{kT}\right) \tag{1}$$

where I is the intensity of the transition, S is the Hönl−London factor, E_{rot} is the ground-state rotational energy, T is the temperature, and k is the Boltzmann constant. A linear fit to the plot of the natural logarithm divided by the Hönl−London factor[33] for that transition, S, versus the ground-state rotational energy, E_{rot}, yields a slope that is inversely proportional to the temperature multiplied by the Boltzmann constant. Analysis of the experimental data in Figure 6a, a room-temperature NO sample, results in a fitted temperature of 295 ± 6 K and validates the methodology of using spectral intensities for determining rotational temperatures.

Figure 10 contains Boltzmann plots of the ground-state energies of the NO photoproduct from the photodissociation of $Co(CO)_3NO$, separated by branch. Due to degeneracies, the spectrum separates into 8 distinct branches, P_{11}, $Q_{11} + P_{12}$, $Q_{12} + R_{11}$, R_{12}, P_{21}, $Q_{21} + P_{22}$, $Q_{22} + R_{21}$, and R_{22}, from the 12 allowed transitions. Two of the branches (P_{11} and P_{21}) were not resolvable into individual transitions, so those do not appear in Figure 10. A two-temperature fit to the data gives rotational temperatures of 580 ± 70 K for $E_{rot} < 500$ cm^{-1} and 2800 ± 300 K for $E_{rot} > 500$ cm^{-1} for the two distributions.

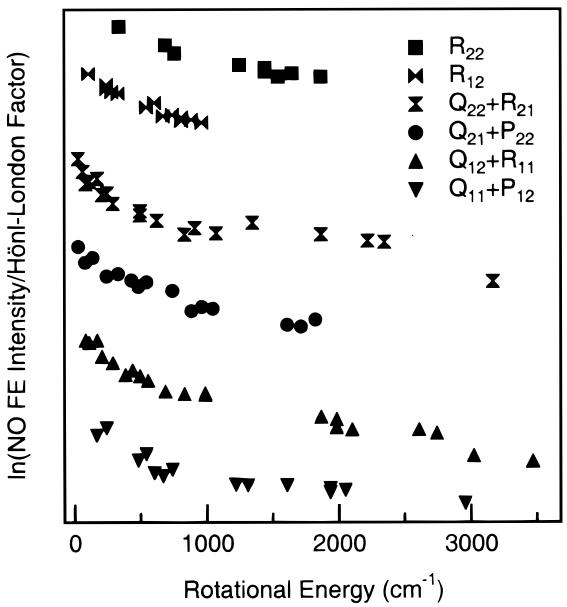

Figure 10. Boltzmann plots of NO fluorescence excitation from the photodissociation of $Co(CO)_3NO$, separated by branch.

A second temperature determination was performed to eliminate any questions regarding saturation or product state alignment effects in the analysis of the branches in the NO FE spectrum. In an analysis similar to that described by Georgiou and Wight,[4,34] two spectra arising from the same laser and detection parameters are compared, the NO FE spectrum from the photodissociation of $Co(CO)_3NO$ and the room-temperature NO FE spectrum. The room-temperature NO FE spectrum is assumed to follow Boltzmann statistics. The rotational population of NO in the photodissociation experiment is determined by

$$N(J,T) = (2J+1)\exp\left(-\frac{E_{rot}}{kT}\right) = \left(\frac{I}{I'}\right)(2J+1)\exp\left(-\frac{E_{rot}}{kT'}\right) \tag{2}$$

where I is the NO FE intensity of a feature in the photodissociation experiment, I' is the intensity of the line in the room-temperature NO FE spectrum, J is the rotational level in the ground state, T' is assumed to be 295 K for the room-temperature sample, and $N(J,T)$ is the adjusted population. Normalizing the photodissociation spectrum by the room-temperature NO FE spectrum removes modest saturation or product-state alignment effects. A plot similar to Figure 10, for the adjusted population, yields rotational temperatures of the NO photoproducts of 570 ± 40 K for $E_{rot} < 500$ cm^{-1} and 2600 ± 800 K for $E_{rot} > 500$ cm^{-1}, which agree with the separate Boltzmann determination above.

These data are not fit well by a single line. A possible explanation is that there are two separate NO rotational distributions resulting from two separate photodissociation mechanisms. The apparent two-photon power dependence in Figure 8 suggests that the photodissociation mechanism begins with the absorption of one photon. The excited molecule then dissociates by two different pathways, each producing NO that

is probed by a second photon. Both pathways for producing NO follow Boltzmann statistics, representing two separate linear fits to the data. Two origins for the different photodissociation pathways are proposed. First, the order of ligand dissociation affects the available energy when the NO dissociates. Less energy is available to the NO ligand as the number of CO ligands dissociated increases prior to the NO dissociation. Second, there is less excess energy available within the dissociating molecule and fragments if the dissociation follows the spin-conserved doublet channel because the dissociation is asympototically linked to the lowest energy doublet state ($a^2F_{7/2}$) in Co, 7442.41 cm^{-1} above the ground state ($a^4F_{9/2}$).

The current data imply higher rotational temperatures than the results of Georgiou and Wight, who reported rotational temperatures for NO of 450 ± 150 and 1400 ± 150 K following the photodissociation of $Co(CO)_3NO$ in the same wavelength range.[4] Qualitatively, both sets have similar appearance in that different portions of the Boltzmann plot are best fit by two separate straight lines. Quantitatively, the disagreement in the temperatures found may arise from the differences in laser intensities (e.g., in the REMPI experiments the laser beam was focused to a small spot diameter, but in the FE experiments the beam was not focused) or in the initial state preparation (e.g., Georgiou and Wight's effusive beam versus the free jet expansion conditions of these experiments).

V. Summary and Conclusions

The photodissociation of $Co(CO)_3NO$ near 225 nm was studied by emission spectroscopy. One photoproduct, NO, has two apparent rotational distributions, leading to two rotational temperatures, 580 ± 70 K for $E_{rot} < 500$ cm^{-1} and 2800 ± 300 K for $E_{rot} > 500$ cm^{-1}. These temperatures are higher than the previously reported values from a REMPI study of $Co(CO)_3NO$ in the same spectral region. A second photoproduct, a bare Co atom, is left with a significant amount of electronic energy following an apparent two-photon complete dissociation of $Co(CO)_3NO$. The nascent Co* atom emits a 340−360-nm photon, and assignments have been made to 16 separate Co emission branches. Analysis of the relative intensities of the individual Co* emission lines indicates that the product states cannot be fit to a single Boltzmann temperature, although individual *J* states within a particular LS configuration are statistically populated. Photodissociation at 221.5 nm forms a higher population of quartet states in Co*, relative to doublet states. Use of the highest energy excited state permits an estimation of the upper limit for the average BDE in $Co(CO)_3NO$, 36.2−38.6 kcal/mol for adiabatic dissociation to the ground state of Co ($a^4F_{9/2}$) and 41.2−43.9 kcal/mol for diabatic dissociation to the lowest-lying Co doublet state ($a^2F_{7/2}$). Although these values are larger than would be expected from previous studies of first-row transition-metal carbonyl BDEs, it is not surprising because a metal−NO bond is stronger than a metal−CO bond.

Acknowledgment. J.A.B. gratefully acknowledges the support of the Pew Midstates Science and Mathematics Consortium for fellowship support. T.O.F. and R.G.B. thank the Pew Midstates Science and Mathematics Consortium for Undergraduate Scholar Awards. This work was supported by National Science Foundation Grant CHE-9157713 and by an equipment grant from Dow-Corning Corporation.

References and Notes

(1) Evans, W.; Zink, J. I. *J. Am. Chem. Soc.* **1981**, *103*, 2635.
(2) Rayner, D. M.; Nazran, A. S.; Drouin, M.; Hackett, P. A. *J. Phys. Chem.* **1986**, *90*, 2882.
(3) Wang, W.; Chen, F.; Lin, J.; She, Y. *J. Chem. Soc., Faraday Trans.* **1995**, *91*, 847.
(4) Georgiou, S.; Wight, C. A. *J. Chem. Phys.* **1989**, *90*, 1694.
(5) Georgiou, S.; Wight, C. A. *J. Phys. Chem.* **1990**, *94*, 4935.
(6) Prinslow, D. A.; Niles, S.; Wight, C. A.; Armentrout, P. B. *Chem. Phys. Lett.* **1990**, *168*, 482.
(7) Niles, S.; Prinslow, D. A.; Wight, C. A.; Armentrout, P. B. *J. Chem. Phys.* **1990**, *93*, 6186.
(8) Hellner, L.; Masanet, J.; Vermeil, C. *Chem. Phys. Lett.* **1981**, *83*, 474.
(9) Karny, Z.; Naaman, R.; Zare, R. N. *Chem. Phys. Lett.* **1978**, *59*, 33.
(10) Jackson, R. L.; Tyndall, G. W. *Chemtronics* **1989**, *4*, 127.
(11) Jackson, R. L. *Chem. Phys. Lett.* **1989**, *163*, 315.
(12) Jackson, R. L. *Acc. Chem. Res.* **1992**, *25*, 581.
(13) Jackson, R. L. *J. Chem. Phys.* **1992**, *96*, 5938.
(14) Tyndall, G. W.; Jackson, R. L. *J. Am. Chem. Soc.* **1987**, *109*, 582.
(15) Tyndall, G. W.; Jackson, R. L. *J. Chem. Phys.* **1988**, *89*, 1364.
(16) Tyndall, G. W.; Larson, C. E.; Jackson, R. L. *J. Phys. Chem.* **1989**, *93*, 5508.
(17) Tyndall, G. W.; Jackson, R. L. *J. Phys. Chem.* **1991**, *95*, 687.
(18) Buntin, S. A.; Cavanagh, R. R.; Richter, L. J.; King, D. S. *J. Chem. Phys.* **1991**, *94*, 7937.
(19) Waller, I. M.; Hepburn, J. W. *J. Chem. Phys.* **1988**, *88*, 6658.
(20) Waller, I. M.; Davis, H. F.; Hepburn, J. W. *J. Phys. Chem.* **1987**, *91*, 506.
(21) Schlenker, F. J.; Bouchard, F.; Waller, I. M.; Hepburn, J. W. *J. Chem. Phys.* **1990**, *93*, 7110.
(22) Mallard, W. G.; Miller, J. H.; Smity, K. C. *J. Chem. Phys.* **1982**, *76*, 3483.
(23) Herzberg, G. *Molecular Spectra and Molecular Structure I. Spectra of Diatomic Molecules*, 2nd ed.; Krieger: Malabar, FL, 1950.
(24) Calvert, J. G.; Pitts, J. N. *Photochemistry*; Wiley: New York, 1966.
(25) Sugar, J.; Corliss, C. *J. Phys. Chem. Ref. Data* **1985**, *14*, 513.
(26) Sunderlin, L. S.; Wang, D.; Squires, R. R. *J. Am. Chem. Soc.* **1992**, *114*, 2788.
(27) Sunderlin, L. S.; Weng, D.; Squires, R. R. *J. Am. Chem. Soc.* **1993**, *115*, 12060.
(28) Goebel, S.; Haynes, C. L.; Khan, F. A.; Armentrout, P. B. *J. Am. Chem. Soc.* **1995**, *117*, 6994.
(29) Wight, C. A.; Armentrout, P. B. In *Laser Chemistry of Organometallics*; Chaiken, J., Ed.; ACS Symposium Series 530; American Chemical Society: Washington, DC, 1993; p 61.
(30) Hsiao, Y.; Niederkofler, E. E.; Coppin, S. M.; Adams, J. L.; Reichert, E. L.; Bartz, J. A. To be published.
(31) Fenske, R. F.; Jensen, J. R. *J. Chem. Phys.* **1979**, *71*, 3374.
(32) Collman, J. P.; Hegedus, L. S.; Norton, J. R.; Finke, R. G. *Principles and Applications of Organotransition Metal Chemistry*; University Science Books: Mill Valley, CA, 1987.
(33) Earls, L. T. *Phys. Rev.* **1935**, *48*, 423.
(34) Georgiou, S.; Wight, C. A. *J. Chem. Phys.* **1988**, *88*, 7418.